第 32卷 第 5期 焊 接 学 报 Vol.32 No.5
2011年 5月 TRANSACTIONS OF THE CHINA WELDING INSTITUTION May 2011

拘束控制铝合金焊接面外变形行为分析

肖晓明[1]， 彭 云[1]， 张建勋[2]， 裴 怡[2]， 田志凌[1]
（1. 钢铁研究总院 先进钢铁流程及材料国家重点实验室，北京 100081；
2. 西安交通大学 金属材料强度国家重点实验室，西安 710049）

肖晓明

摘 要：利用温度和变形实时测量系统，对 5A12铝合金板拘束焊变形和外拘束力进行了试验研究，分析了拘束力大小和拘束释放对试板面外变形的影响．结果表明，施加不同的拘束力，试板焊后残余面外变形大小不同，适当的拘束可以有效地控制焊接变形；焊接结束拘束卸载后，焊接件变形出现不同程度的反弹；弹性回复是造成拘束焊残余变形的主要因素；拘束力大小为 0.2 kN，采用对称面压紧的方式，拘束位置距焊缝中心 45 mm，厚度为 6 mm的 5A12铝合金试板残余变形最小．

关键词：铝合金；变形；拘束力；弹性回复
中图分类号：TG115.28 文献标识码：A 文章编号：0253－360X(2011)05－0033－04

0 序 言

铝合金因具有良好的耐蚀性、较高的比强度和比刚度、好的导电性及导热性等优点，广泛应用于航空航天领域．但由于铝合金焊接变形较大，因而对铝合金结构焊接变形的预测和控制是焊接领域亟待解决的重要问题．常用的控制薄板焊接变形的工艺措施有刚性固定法、反变形法、预拉伸法等．刚性固定法（拘束焊），即采用设计合理的夹具，将焊件固定起来进行焊接，增加其刚性，达到减小焊接变形的目的．已有研究结果表明，采用合理的夹具布置可以很好地控制焊接变形[1]．外拘束是影响焊接应力和变形的重要因素，拘束对焊接应力变形的影响规律以及如何对焊接件进行合理拘束是焊接领域特别是薄板焊接和焊接装配的一个值得研究的方面．国内外的许多学者在拘束与焊接变形的关系方面做了大量的研究工作．Cronje[2]讨论了拘束对低碳钢薄板焊接变形的影响，研究结果表明，拘束增加，变形减小，但残余应力变大．Mahapatra等人[3]研究了拘束对埋弧焊接角变形的影响，结果发现拘束能显著减少焊接角变形．Wahab等人[4]分别用数值模拟和试验的方法分析了保证焊件不变形的拘束力大小，以及焊接速度和热输入对拘束力的影响．徐文利等人[5]从力学（拘束力）角度出发，通过调整焊接温度场，控制焊缝及近缝区应力应变发展，实现了高强铝合金 LY12CZ薄板的低应力小变形无热裂焊接．贾迎军等人[6]利用有限元法对拘束焊进行了模拟分析，通过对不同厚度钢板拘束焊问题的研究，计算出最优的拘束力和拘束长度（拘束位置）．作者采用焊接温度、变形测量系统[7,8]，对 5A12铝合金试板拘束焊接变形的行为进行试验研究．分析了拘束焊接变形曲线的特点、不同拘束力下 5A12铝合金板变形情况以及拘束力卸载对焊接残余变形的影响．

1 试验方法

采用 5A12铝合金作为试验材料，焊件尺寸为 200 mm×160 mm×6 mm，试验装置见图 1．如图 1所示，采用 1号位移传感器和 2号位移传感器对距焊缝中心 90 mm处 C点和 D点的焊接面外变形进行测量．两个力传感器对称分布，拘束方式为面压紧，压板距焊缝中心 45 mm．焊接方法为钨极氩弧

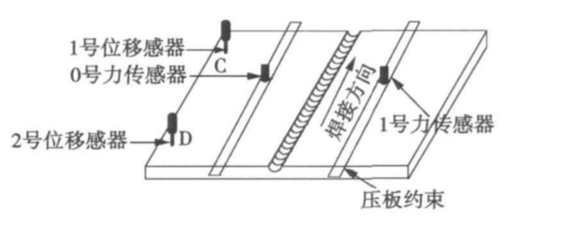

图 1 铝合金试验安排示意图
Fig. 1 Schematic representation of experimental setup

收稿日期：2010－01－12
基金项目：国家自然科学基金资助项目（50875200）；博士点基金资助项目（20070698088）

焊，由焊接机器人协助完成，在试板中心沿图 1所示方向进行堆焊.

焊接工艺参数是：焊接电流 150 A，焊接速度 12 cm/min，氩气流量 10 L/min，电弧电压 14 V，焊接环境温度为 20 ℃. 采用动态测量系统对焊接变形和拘束力进行实时测量，其中变形和拘束力的测量选用体积较小的电感调频式 BWG3－20 mm位移传感器和 H3力传感器.

2 试验结果及分析

2.1 焊接面外变形动态过程

试板施加单端拘束，拘束力变化曲线见图 2. 不施加拘束端 C点、D点面外变形随时间变化趋势曲线如图 3所示. 由图 2可知，焊接开始时通过 1号力传感器预加力 0.56 kN. 0～80 s为焊接加热阶段，80 s以后为冷却阶段. 随着焊接加热过程的进行，试板温度陡增，焊后试板逐渐冷却，热胀冷缩导致拘束力亦呈先增后降趋势. 试板冷却到室温后，拘束力趋于稳定. 由图 3可见，焊接开始后，变形迅速增加，这是由于随着焊接电弧的移动，电弧后面的

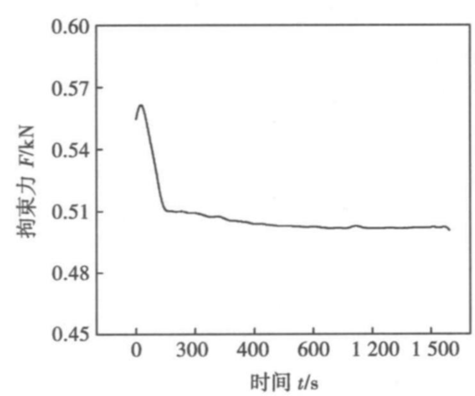

图 2 动态拘束力曲线

Fig. 2 Curve of dynamic force

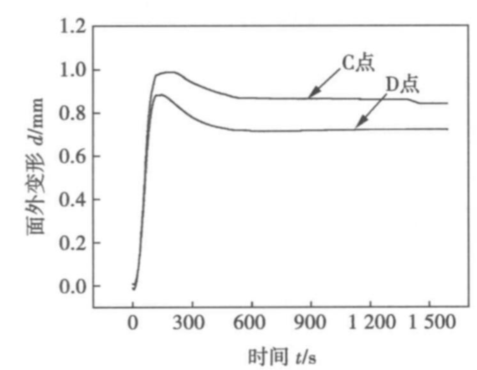

图 3 动态变形曲线

Fig. 3 Curves of dynamic out-of-plane distortion

焊缝金属开始冷却，发生横向收缩，导致试板上翘. 焊后，随着试板慢慢冷却，变形稍有减小，并逐渐趋于稳定，表现为残余变形量. C点残余变形量约为 0.86 mm，D点残余变形量约为 0.72 mm.

试板施加双端对称拘束（拘束焊），拘束力分别为 0.1，0.2，0.5，0.8 kN. 焊接结束后，试板温度降至室温，左侧拘束卸载，通过位移传感器观察 C点、D点面外变形情况. 图 4和图 5分别为拘束力和 C点面外变形随时间的变化趋势曲线. 由图 4可知，焊接过程中拘束力变化不明显，在冷却阶段均有少许下降，但很快趋于稳定. 由图 5可见不同拘束力下试板面外变形曲线趋势相同. 焊接开始后，变形迅速增加，不同拘束力下试板最大变形量有所不同. 焊接结束后，试板冷却，变形减小，试板达到平衡温度后，变形趋于稳定. 较之单端拘束，试板变形较小，且不同拘束力对变形控制效果不同. 试板冷却到室温，左侧拘束卸载，由于弹性回复，变形迅速增加，表现为残余变形量. 拘束力为 0.8 kN试板残余变形最大，拘束力为 0.2 kN试板残余变形最小.

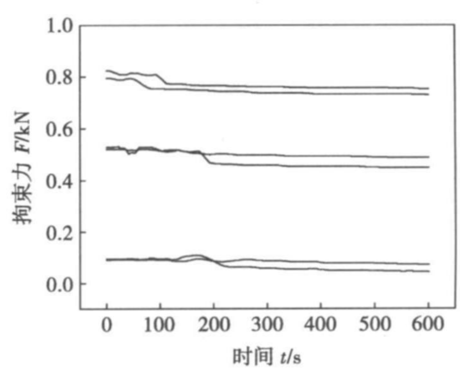

图 4 拘束焊动态拘束力曲线

Fig. 4 Dynamic force curves of restraint welding

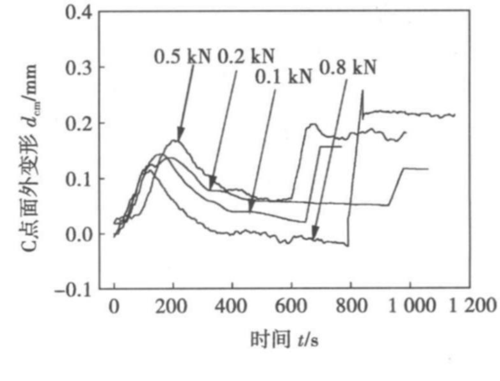

图 5 拘束焊动态变形曲线

Fig. 5 Dynamic distortion curves of constrain welding

图 6为单端拘束和双端拘束面外变形曲线对

比. 由图 6可知两者存在明显的区别,施加拘束焊接变形显著减小. 随着焊接加热过程的进行,单端拘束焊接变形持续增加,随后试板冷却变形有少许下降,但很快趋于稳定,表现为残余变形. 故单端拘束变形曲线可分为 3个阶段,变形增加阶段、变形减少阶段及稳定阶段. 双端拘束焊接变形在加热阶段变形同样持续增加,但变形较小,焊后随着试板冷却变形减至较小. 当试板冷却到室温,拘束释放,由于弹性回复造成变形迅速增加,但残余变形量远远小于单端拘束. 故双端拘束变形曲线可分为 4个阶段,变形增加阶段、变形减少阶段、稳定阶段及弹性回复阶段.

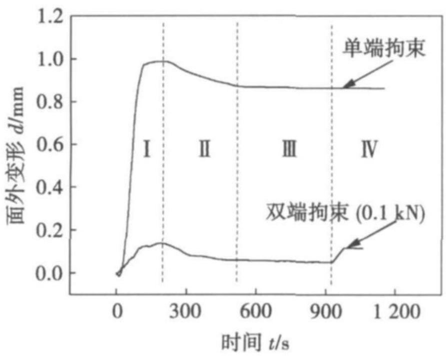

图 6　焊接动态变形曲线
Fig. 6　Dynamic distortion curves of welding

2.2　拘束力大小对焊接面外变形的影响

试板在各不同拘束力下的焊接残余变形如表 1所示. 从表中可以看出,试板在不同拘束力下均发生了不同程度的变形,不施加拘束时,变形现象最严重.

表 1　拘束力及其对应的焊接残余变形
Table 1　Restraining force and residual distortion

拘束力 F/kN	C点残余变形 d_{CC}/mm	D点残余变形 d_{DC}/mm
0	0.86	0.72
0.1	0.16	0.22
0.2	0.12	0.13
0.5	0.18	0.21
0.8	0.22	0.25

图 7为 1号位移传感器所测 C点在不同拘束力下的残余变形情况. 由图 7可知,不施加拘束试板残余变形最大 (0.85 mm). 施加双端对称拘束,拘束力为 0.1 kN时,残余变形迅速减小. 拘束力为 0.2 kN时,残余变形最小 (0.18 mm). 但是随着拘束力的继续增加,残余变形又呈缓慢上升趋势,在 0.8 kN拘束力下其残余变形达到 0.25 mm. 这是因为焊接过程中产生的不均匀塑性变形是引起试板变形和应力的主要因素. 在不施加拘束的情况下,试板焊接变形明显. 施加拘束,控制了焊接变形,但增大了试板内部应力,尤其是拘束施加部位. 拘束过大,应力增加,拘束卸除后由于拘束施加处应力释放焊接变形较适当拘束情况下稍有增加.

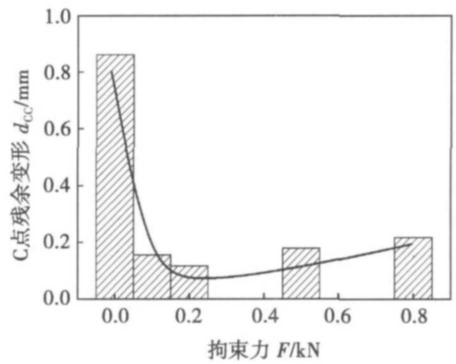

图 7　C点残余变形
Fig. 7　Residual distortion of point C

图 8为 2号位移传感器所测 D点在不同拘束力下的残余变形情况,其趋势与图 7相同. 由此可知,施加适当的拘束可以有效的控制焊接变形. 对于 6 mm厚 5A12铝合金板,采用对称面压紧的方式,拘束位置距焊缝中心 45 mm,最优化的拘束力应控制在 0.2 kN左右.

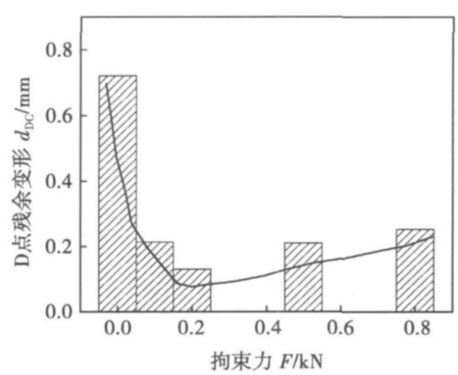

图 8　D点残余变形
Fig. 8　Residual distortion of point D

2.3　拘束释放对焊接面外变形的影响

拘束释放后,焊接变形有不同程度的反弹. 拘束力不同,焊接变形在拘束释放后的反弹不同. 图 9及图 10为不同大小初始拘束力作用在距焊缝相同位置时,拘束卸载前后的变形情况以及卸载拘束前后的变形差值 (焊接件拘束释放后的弹性回复,图中阴影部分). 如图 9和图 10所示,当拘束力为 0.2

kN时焊接件残余变形最小,拘束力过小或过大控制变形效果均不好. 在拘束释放前, 0.2 kN拘束力下的焊接变形并非最小, 但拘束释放后, 0.2 kN拘束力下焊接件的弹性回复最小,因而对残余变形的控制效果最好. 由此可知,造成拘束焊残余变形的主要因素是拘束力卸除后的弹性回复,适当的拘束可以减小弹性回复,进而实现控制焊接变形的目的.

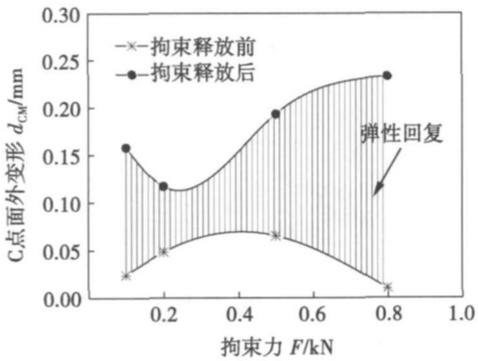

图 9 C 点拘束卸载前后面外变形及弹性回复比较

Fig. 9 Comparisons of spring back and out-of-plane distortion before and after restraints release at point C

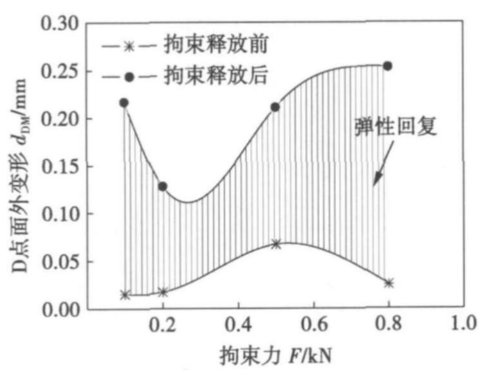

图 10 D 点拘束卸载前后面外变形及弹性回复比较

Fig. 10 Comparisons of spring back and out-of-plane distortion before and after restraints release at point D

3 结 论

(1) 单端拘束焊接变形曲线和双端拘束焊接变形曲线存在明显的区别,双端拘束焊接变形曲线存在弹性回复阶段.

(2) 在焊接过程中施加拘束是一种有效的主动控制焊接变形的方式. 焊接变形控制存在最优拘束值,对于 6 mm厚 5A12铝合金试板,采用所选拘束方式,最佳的拘束力为 0.2 kN.

(3) 拘束力不同时,卸力后的残余变形大小不同. 造成拘束焊残余变形的主要因素是拘束卸除后的弹性回复,适当的拘束可以减小弹性回复,进而实现控制焊接变形的目的.

参考文献:

[1] 张建强, 赵海燕, 鹿安理, 等. 夹具约束对铝合金薄板焊接变形的影响[J]. 稀有金属材料与工程, 2009, 38(3): 165—169.
Zhang Jianqiang, Zhao Haiyan, Lu Anli, et al. Effects of clamps on welding distortion in thin aluminum alloy plate[J]. Rare Metal Materials and Engineering, 2009, 38(3): 165—169.

[2] Cronje M. Finite element modeling of shielded metal arc welding[D]. Matieland, South Africa: Stellenbosch University, 2005.

[3] Mahapatra M M, Datta G L, Pradhan B, et al. Three-dimensional finite element analysis to predict the effects of SAW process parameters on temperature distribution and angular distortions in single-pass butt joints with top and bottom reinforcements[J]. International Journal of Pressure Vessels and Piping, 2006, 83: 721—729.

[4] Wahab M A, Alam M S, Painter M J. Experimental and numerical simulation of restraining forces in gas metal arc welded joints[J]. Welding Journal, 2006, 85(2): 35—43.

[5] 徐文立, 刘雪松, 方洪渊, 等. 薄板高强铝合金 LY12CZ焊接工艺参数的优化[J]. 焊接学报, 2004, 25(2): 39—42.
Xu Wenli, Liu Xuesong, Fang Hongyuan, et al. Parameters optimization for welding aluminum alloy 2024 sheet with high strength[J]. Transactions of the China Welding Institution, 2004, 25(2): 39—42.

[6] 贾迎军, 蔺海荣, 李文娟. 拘束焊接头应力应变的数值计算[J]. 山东建筑大学学报, 2006, 21(4): 321—324.
Jia Yingjun, Lin Hairong, Li Wenjuan. The numerical calculation of stress and strain in restraint welding joints[J]. Journal of Shandong Jianzhu University, 2006, 21(4): 321—324.

[7] 王 蕊, 张建勋, 梁振新. 新型焊接变形与热循环动态测试系统[J]. 焊接, 2006(1): 27—31.
Wang Rui, Zhang Jianxun, Liang Zhenxin. A new measuring system for welding dynamic distortion and thermal cycle[J]. Welding & Joining, 2006(1): 27—31.

[8] 王 蕊, 张建勋, 梁振新. 铝合金氩弧焊接角变形动态过程表征[J]. 焊接学报, 2007, 28(3): 29—32.
Wang Rui, Zhang Jianxun, Liang Zhenxin. Characteristics of dynamic welding angular distortion of an aluminum alloy with TIG welding[J]. Transactions of the China Welding Institution, 2007, 28(3): 29—32.

作者简介: 肖晓明, 女, 1983年出生, 博士. 主要从事钢铁焊接材料及焊接性研究工作. 发表论文 2篇. Email: gyxxm99@yahoo.com.cn

通讯作者: 张建勋, 男, 教授, 博士研究生导师. jxzhang@mail.xjtu.edu.cn

100084, China; 2. Key Laboratory for Advanced Materials Processing Technology, The Ministry of Education, Tsinghua University, Beijing 100084, China). p 17-20, 24

Abstract: The effects of welding parameters including laser power, welding speed, welding conditions on pore formation tendency (represented as porosity) during laser welding of die-cast magnesium alloys with two different gas contents were investigated, and the porosity prevention measures were also studied. It is shown that the pore formation tendency during laser welding of 2 mm thick die-cast magnesium alloys with higher gas content is greater than that of 5 mm thick die-cast magnesium alloys with lower gas content. As a whole, the porosity increases with the increase of laser power and the decrease of welding speed for both two thicknesses. For 5 mm thick die-cast magnesium alloys with lower gas content, low porosity weld bead can be obtained by both double sided welding and remelting after welding, and the porosity can reduce to 2.4% and 2.5%, respectively. However, for the 2 mm thick die-cast magnesium alloys, these porosity prevention measures are not effective.

Key words: pore; pore prevention; laser welding; welding parameters; die-cast magnesium alloys

Effect of high-energy shot peening on diffusion behavior of nickel in iron WANG Yuetian, SHENG Guangmin, SUN Jianchun, LU Hao (School of Materials Science and Engineering, Chongqing University, Chongqing 400030, China). p 21-24

Abstract: High-energy shot peening (HESP) was used to make surface self nano-crystallization (SSNC) on pure iron. The thickness of the deformation layer, surface grain size and hardness were characterized by optical microscope (OM), scanning electron microscopy (SEM) and X-ray diffraction analysis (XRD), and then Ni film was penetrated into the surface of iron by the Gleeble 1500 thermal simulation test machine. The SEM was used to compare the diffusion effects. The results showed that the surface of industrial pure iron was refined obviously after the shot peening treatment, its hardness increased significantly and was one time higher than that of the matrix. Under the same conditions, the diffusion rate of Ni in the specimen after SSNC was higher than that without SSNC, so the SSNC technology can improve diffusion effect of Ni on the surface of industry pure iron.

Key words: pure iron; SSNC; shot peening; diffusion

Signal processing in ultrasonic test of austenitic welds based on time-frequency analysis WANG Bingfang, HAN Zandong, YUAN Keyi, CHEN Yifang (Key Laboratory for Advanced Materials Processing Technology, The Ministry of Education, Tsinghua University, Beijing 100084, China). p 25-28

Abstract: Signal processing in ultrasonic test of austenitic welds was studied. Based on time-frequency analysis, a comprehensive signal processing method was proposed, which was a combination of matching pursuit and wavelet analysis. This method distinguishes flaw information and material noise from a point of energy and frequency, respectively, and improves the SNR of the ultrasonic echo signal. To verify the effectiveness of the method, an ultrasonic test system was established. Test experiment was carried out with a 53 mm thick weld specimen, and a signal with large amount of material noise was acquired. The noised signal was processed by the proposed method. The first 18 time-frequency atoms were extracted by matching pursuit with sym8 wavelet packet dictionary, the extracted signal was analyzed by sym8 wavelet decomposition and reconstructed with low frequency coefficients. The result shows that the material noise is reduced effectively and the flaw echo signal is enhanced significantly.

Key words: austenitic welds; ultrasonic test; time-frequency analysis; matching pursuit; wavelet analysis

Analysis on growth mechanism on interfacial interlayer on Fe/Al couple WU Mingfang[1,2], SI Naichao[1], WANG Jing[2], WANG Fengjiang (1. School of Materials Science and Engineering, Jiangsu University, Zhenjiang 212013, China; 2. School of Materials Science and Engineering, Jiangsu University of Science and Technology, Zhenjiang 212003). p 29-32

Abstract: To understand the formation mechanism and growth behavior of Fe-Al intermetallics, the element diffusion and interfacial reactive interlayer in Fe/Al couple were studied at the different heating temperature and holding time. The interfacial structure is $Fe/FeAl_x + Al/FeAl/Al$ at the shorter holding time, while the unstable $FeAl_x$ and FeAl will change into the stable Fe_2Al_5 and $FeAl_3$ intermetallics at a longer holding time. The final interfacial structure was $Fe/Fe_2Al_5 + FeAl_3/Al$. The growth of interfacial reactive layer follows the parabolic rule, and its rate is controlled by the diffusion rate of Fe atoms into Al side. The results are helpful to improve the bonding quality between aluminum alloys and stainless steel.

Key words: Fe; Al; diffusion; interfacial structure

Investigation of out-of-plane welding distortion in aluminum alloy welding with external restraint XIAO Xiaoming[1], PENG Yun[1], ZHANG Jianxun[2], PEI Yi[1], TIAN Zhiling (1. State Key Laboratory of Advanced Steel Processes and Products, Central Iron & Steel Research Institute, Beijing 100081, China; 2. State Key Laboratory for Mechanical Behavior of Materials, Xi'an Jiaotong University, Xi'an 710049, China). p 33-36

Abstract: The characteristics of constraint force and dynamic welding distortion of aluminum alloy 5A12 with constraint TIG welding were investigated by dynamic temperature and distortion measuring system. The effects of constraint force and its release on out-of-plane welding distortion were analyzed. Research results show that out-of-plane welding distortion is different with the different constraint force, and welding distortion can be controlled by the proper constraint force, the welding distortion will rebound to some extent after the constraint force being released, which is the main factor to result in the residual distortion of constraint welding, the residual distortion of 6 mm thick aluminum alloy 5A12 plate can be well restrained at the constraint force of 0.2 kN and the loading position is 45 mm form the centerline of weld.

Key words: aluminum alloy; deformation; constraint force; elastic recovery

Double-pulsed MIG expert database based on mathematical modeling CHEN Xiaofeng, LIN Fang, WEI Zhonghua, XUE Jiaxiang (School of Mechanical & Automotive Engineering, South China University of Technology, Guangzhou 510640, China). p 37-40